Inorg. Chem. **2006**, *45*, 636–643

Syntheses and Structures of Dinuclear Double-Stranded Helicates of Divalent Manganese, Iron, Cobalt, and Zinc

Stuart D. Reid, Alexander J. Blake, Claire Wilson, and Jason B. Love*

School of Chemistry, University Park, University of Nottingham, Nottingham NG7 2RD, U.K.

Received August 22, 2005

The syntheses and solid-state and solution structures of a series of unusually volatile, charge neutral, [4 + 4] double-stranded helical complexes of divalent manganese, iron, cobalt, and zinc are described. Deprotonation of the N_4-donor iminopyrrole ligand H_2L by KH cleanly generates the salt $K_2(THF)_2L$, which displays both σ and π interactions between K and iminopyrrolyl fragments in the X-ray crystal structure. Transamination, salt elimination, and protonolysis reactions were found to be versatile and, in general, high-yielding routes to the dinuclear double helicates $[M_2(L)_2]$ (M = Mn, Fe, Co, and Zn). These compounds are isomorphous in the solid state by X-ray crystallography and adopt dinuclear cleft motifs as a result of π stacking between opposing iminopyrrolyl fragments. This motif was also observed in the solution structures of $[Fe_2(L)_2]$ and $[Zn_2(L)_2]$ below 230 and 200 K, respectively ($\Delta G^{\ddagger} = \sim 46$ and 39.0 kJ mol^{-1}, respectively).

Introduction

Of the increasing number of known supramolecular architectures, the metallohelicate conveys a historical and fundamentally informative perspective, because since the observation of the first trimetallic, double-stranded helicate, many of the processes involved in the spontaneous assembly of these, and other, intricate systems have become increasingly understood.[1,2] Of the factors integral to helicate formation, the geometric preferences of the metal and the group that separates and links the donor atoms of the ligand are particularly influential. Ligands based upon diphenylmethane-linked iminopyridines **I** (see Chart 1) can form dinuclear double-stranded helicates,[3,4] mixtures of double-stranded helicates and mesocates,[5,6] or solely mesocates[7] when coordinated to tetrahedral Cu^I and Ag^I, but when coordinated to metals that exhibit a preference for octahedral geometries, they form exclusively the triple-stranded helicate.[7−9] Furthermore, the zigzag nature of the aliphatic spacer in the dicatecholate ligands **II** allows control of the synthesis of cationic, dinuclear, triple-stranded, titanium

Chart 1. Some Ligands Used in the Synthesis of Double- and Triple-Stranded Helicates

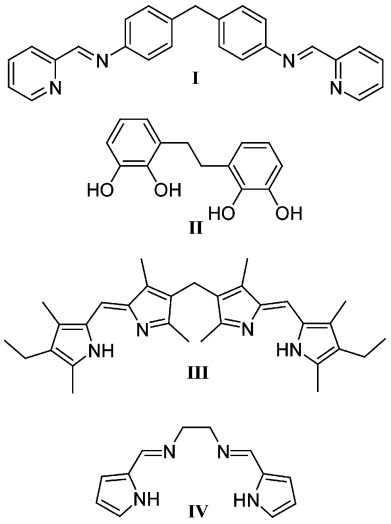

* To whom correspondence should be addressed. E-mail: jason.love@nottingham.ac.uk. Tel: +44 115 8499332. Fax: +44 115 9513563.

(1) Albrecht, M.; Janser, I.; Fröhlich, R. *Chem. Commun.* **2005**, 157.
(2) Albrecht, M. *Chem. Rev.* **2001**, *101*, 3457, Lehn, J.-M. *Supramolecular Chemistry*; VCH: New York, 1995, Lehn, J.-M.; Rigault, A.; Siegel, J.; Harrowfield, J.; Chevrier, B.; Moras, D. *Proc. Natl. Acad. Sci. U.S.A.* **1987**, *84*, 2565, Piguet, C.; Bernardinelli, G.; Hopfgartner, G. *Chem. Rev.* **1997**, *97*, 2005. Piguet, C.; Borkovec, M.; Hamacek, J.; Zeckert, K. *Coord. Chem. Rev.* **2005**, *249*, 705.
(3) Hannon, M. J.; Painting, C. L.; Alcock, N. W. *Chem. Commun.* **1999**, 2023.
(4) Sun, W.-H.; Zhang, T.; Wang, L.; Chen, Y.; Froehlich, R. *J. Organomet. Chem.* **2004**, *689*, 43.
(5) Childs, L. J.; Pascu, M.; Clarke, A. J.; Alcock, N. W.; Hannon, M. J. *Chem.—Eur. J.* **2004**, *10*, 4291.
(6) Lavalette, A.; Tuna, F.; Clarkson, G.; Alcock, N. W.; Hannon, M. J. *Chem. Commun.* **2003**, 2666.
(7) Keegan, J.; Kruger, P. E.; Nieuwenhuyzen, M.; Martin, N. *Cryst. Growth Des.* **2002**, *2*, 329. Cheng, H.; Chun-ying, D.; Chen-jie, F.; Qing-jin, M. *Dalton Trans.* **2000**, 2419.

10.1021/ic051433b CCC: $33.50
Published on Web 12/14/2005

helicates because when an even number of CH_2 spacers are used, helicates are generated, whereas mesocates are formed preferentially when an odd number of CH_2 units are employed.[1]

Despite the ongoing research into the metallohelicate, few examples exist of *neutral* compounds that adopt helical topologies. Notable exceptions are dinuclear complexes of the linked dipyrromethenes **III**,[10] in which the formation of mono- and dinuclear double-stranded helicates has been found to be dependent on the length of the alkyl spacer between the two dipyrromethene N-donor groups,[11] and also the linked iminopyrroles **IV**,[12−14] which have been shown to promote the formation of not only dinuclear double-stranded helicates but also triangles and squares.[15] Furthermore, a neutral dimanganese helicate supported by an analogous linked iminopyrrole ligand has been shown to reorganize upon reaction with O_2 to form a nonhelical complex in which the two manganese ions are bridged by a partially hydrated peroxide ligand.[16]

We have shown previously that the multidentate iminopyrrole ligands, H_2L, which are related to both the above linked dipyrromethenes and linked iminopyrroles, are straightforwardly synthesized in a two-step procedure from readily available dipyrromethanes.[17] We have shown that upon deprotonation of H_2L^{Ph} by KH (where H_2L^{Ph} has diphenyl substitution of the meso carbon) iminopyrrolyl coordination of potassium was preferred over pyrrolyl−pyrrolyl coordination, presumably because of the extension of π conjugation that occurs when the imine N═C bond is coplanar to the pyrrolyl ring. It was also noted that the ability of the two pyrrolyl groups to adopt an anti configuration at the relatively flexible, sp^3-hybridized meso carbon should promote helicate formation. Indeed, we recently communicated that transamination reactions between H_2L and iron(II) and manganese(II) amides generate solely the neutral, dinuclear double-stranded helicates $[M_2(L)_2]$ (M = Fe, Mn), which are unusual in that they are both volatile and display dinuclear cleft motifs in the solid state.[18] We report here full details of both transamination and salt elimination synthetic routes to the above iron and manganese helicates, extension of these routes to include the synthesis of helical complexes of cobalt and zinc and their characterization by X-ray crystallography, and an assessment of the stability in solution of the dinuclear cleft motif present in the iron and zinc helicates by variable-temperature NMR spectroscopy.

Scheme 1. Synthesis of the Double Helicates $[M_2(L)_2]$

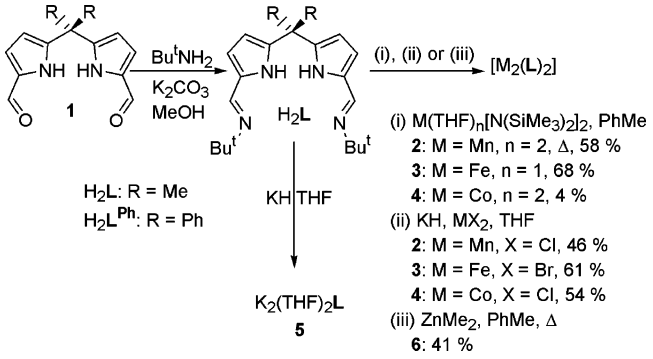

Results and Discussion

Transamination Routes to Dinuclear Helicates. We have shown previously that the transamination reactions between the multidentate iminopyrrole ligand H_2L, prepared by a Schiff-base condensation reaction between the dialdehyde **1** and Bu^{t}NH$_2$ (Scheme 1), and the divalent amido complexes $M(THF)_n[N(SiMe_3)_2]_2$ (M = Mn, Fe) result in the formation of the dinuclear [4 + 4] double helicates $[M_2(L)_2]$ (M = Mn, **2**; M = Fe, **3**).[18] These complexes are unusual in that, unlike the majority of helical complexes, they are charge neutral and volatile and adopt a dinuclear cleft motif in the solid state. We have now found that a similar transamination reaction between the divalent amidocobalt complex $Co(THF)_2[N(SiMe_3)_2]_2$ and H_2L results in the formation of the analogous dicobalt complex $[Co_2(L)_2]$ (**4**), albeit in very low yield (see Scheme 1). The 1:1 ligand-to-metal ratio of **4** is supported by elemental analysis, and the solution magnetic susceptibility, μ_{eff}, of 5.48 μ_B at 298 K is consistent with the presence of two independent $S = {}^3/_2$ high-spin Co^{II} ions (μ_{calc} = 5.12 μ_B). The electron impact mass spectrometry (EIMS) spectrum reveals that **4** exists as a dimer in the gas phase with a molecular ion seen at *m*/*z* 794 (calculated *m*/*z* 794.96); as with the dimanganese and diiron helicates, **2** and **3**, respectively, little or no fragmentation was observed under electron impact conditions.[18] To confirm that **4** adopts a helical structure in the solid state, X-ray diffraction studies were carried out on crystals of **4** that were obtained by slow sublimation at 210 °C and 10^{-2} mbar in a sealed tube. The

(8) Meistermann, I.; Moreno, V.; Prieto, M. J.; Moldrheim, E.; Sletten, E.; Khalid, S.; Rodger, P. M.; Peberdy, J. C.; Isaac, C. J.; Rodger, A.; Hannon, M. J. *Proc. Natl. Acad. Sci. U.S.A.* **2002**, *99*, 5069. Dong, G.; Ke-liang, P.; Chun-ying, D.; Cheng, H.; Qing-jin, M. *Inorg. Chem.* **2002**, *41*, 5978. Hannon, M. J.; Moreno, M.; Prieto, M. J.; Moldrheim, E.; Sletten, E.; Meistermann, I.; Isaac, C. J.; Sanders, K. J.; Rodger, A. *Angew. Chem., Int. Ed.* **2001**, *40*, 880. Yoshida, N.; Ichikawa, K.; Shiro, M. *J. Chem. Soc., Perkin Trans. 2* **2000**, 17. Rodger, A.; Sanders, K. J.; Hannon, M. J.; Meistermann, I.; Parkinson, A.; Vidler, D. S.; Haworth, I. S. *Chirality* **2000**, *12*, 221. Yoshida, N.; Ichikawa, K. *Chem. Commun.* **1997**, 1091.
(9) Hannon, M. J.; Painting, C. L.; Jackson, A.; Hamblin, J.; Errington, W. *Chem. Commun.* **1997**, 1807.
(10) Wood, T. E.; Dalgleish, N. D.; Power, E. D.; Thompson, A.; Chen, X.; Okamoto, Y. *J. Am. Chem. Soc.* **2005**, *127*, 5740. Zhang, Y.; Thompson, A.; Rettig, S. J.; Dolphin, D. *J. Am. Chem. Soc.* **1998**, *120*, 13537.
(11) Thompson, A.; Dolphin, D. *J. Org. Chem.* **2000**, *65*, 7870.
(12) Zhang, G.; Yang, G.; Chen, Q.; Ma, J. S. *Cryst. Growth Des.* **2005**, *5*, 661. Wu, Z.; Yang, G.; Chen, Q.; Liu, J.; Yang, S.; Ma, J. S. *Inorg. Chem. Commun.* **2004**, *7*, 249. Liang, L.-C.; Lee, P.-Y.; Lan, W.-L.; Hung, C.-H. *J. Organomet. Chem.* **2004**, *689*, 947. Yang, L.; Chen, Q.; Li, Y.; Xiong, S.; Li, G.; Ma, J. S. *Eur. J. Inorg. Chem.* **2004**, 1478. Kikuchi, T.; Kabuto, K.; Yokoi, H.; Ixaizumi, M.; Mori, W. *J. Chem. Soc., Chem. Commun.* **1983**, 1306.
(13) Yang, L.-Y.; Chen, Q.-Q.; Yang, G.-Q.; Ma, J.-S. *Tetrahedron* **2003**, *59*, 10037.
(14) van Stein, G. C.; van Koten, G.; Passenier, H.; Steinebach, O.; Vrieze, K. *Inorg. Chim. Acta* **1984**, *89*, 79.
(15) Wu, Z.; Chen, Q.; Xiong, S.; Xin, B.; Zhao, Z.; Jiang, L.; Ma, J. S. *Angew. Chem., Int. Ed.* **2003**, *42*, 3271.
(16) Franceschi, F.; Guillemot, G.; Solari, E.; Floriani, C.; Re, N.; Birkedal, H.; Pattison, P. *Chem.−Eur. J.* **2001**, *7*, 1468.
(17) Love, J. B.; Blake, A. J.; Wilson, C.; Reid, S. D.; Novak, A.; Hitchcock, P. B. *Chem. Commun.* **2003**, 1682.
(18) Reid, S. D.; Blake, A. J.; Köckenberger, W.; Wilson, C.; Love, J. B. *Dalton Trans.* **2003**, 4387.

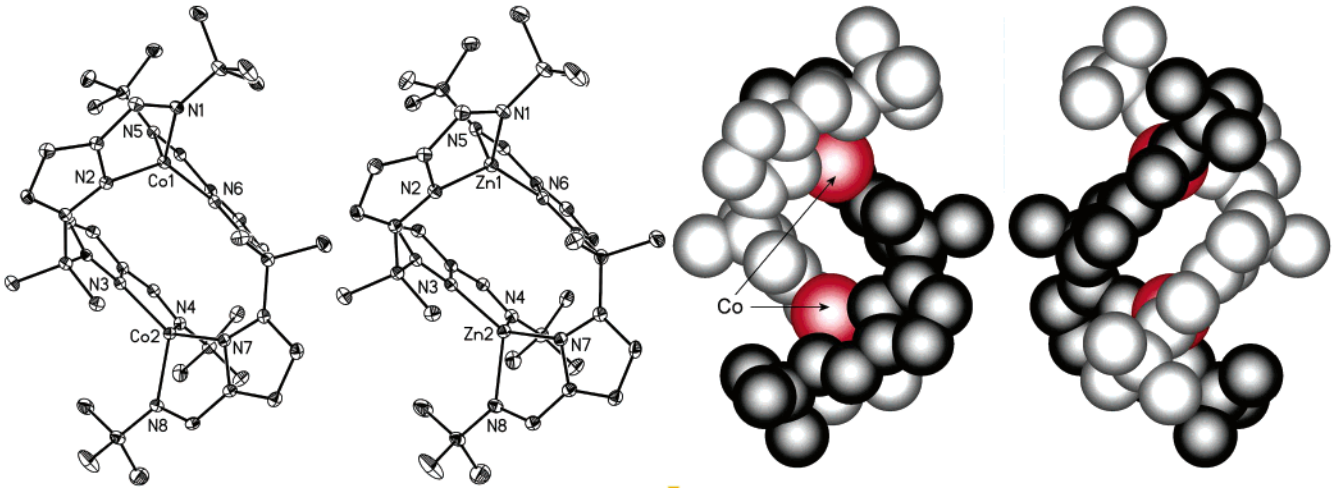

Figure 1. X-ray crystal structures of **4** and **6** (30% thermal ellipsoids; all hydrogens omitted for clarity) and space-filling representation of **4**.

Table 1. Selected Bond Lengths (Å) and Angles (deg) for the Cobalt and Zinc Double Helicates **4** and **6**

$[Co_2(L)_2]_2$ (**4**)		$[Zn_2(L)_2]$ (**6**)	
Co1−N1	2.047(3)	Zn1−N1	2.054(3)
Co1−N2	1.989(3)	Zn1−N2	1.978(3)
Co1−N5	2.055(3)	Zn1−N5	2.068(3)
Co1−N6	1.980(3)	Zn1−N6	1.958(3)
N1−Co1−N2	84.42(10)	N1−Zn1−N2	85.02(10)
N1−Co1−N5	111.71(10)	N1−Zn1−N5	109.96(11)
N1−Co1−N6	126.05(10)	N1−Zn1−N6	125.72(11)
N2−Co1−N5	121.80(10)	N2−Zn1−N5	120.57(11)
N2−Co1−N6	130.67(11)	N2−Zn1−N6	132.08(11)
N5−Co1−N6	85.23(11)	N5−Zn1−N6	85.61(11)

solid-state structure of **4** is shown in Figure 1, with selected bond lengths and angles and crystal data detailed in Tables 1 and 2, respectively.

As with **2** and **3**, the dicobalt complex **4** crystallizes as a racemic mixture of *M* and *P* double-stranded helicates. The Co−Co separation of 4.914 Å is too long for any significant Co−Co orbital overlap and, allied with the presence of the sp^3-hybridized *meso*-CMe_2 linker between the two Co centers that precludes any superexchange pathway, correlates well with the observed room-temperature magnetic susceptibility. The geometries around the metals are similar and are best described as distorted tetrahedral in which, for example, the N2−Co1−N6 angle at 130.67(11)° is more obtuse than the expected tetrahedral angle, although of magnitude similar to those observed previously for the Mn_2 and Fe_2 double helicates **2** and **3**.[18] A similarly obtuse N−Co−N angle of 130.70(9)° was observed in the mixed-metal dipyrrolyl complex $Co_2Fe_2[(C_4H_3N)_2C(c\text{-}C_6H_{11})_2]$,[19] while other expanded angles have been observed for pseudotetrahedral Mn[20] and Fe[19,21] and are presumably a consequence of the constraint proffered by the chelating ligands. The pyrrolic Co−N bond distances, Co1−N2 = 1.989(3) Å and Co1−N6 = 1.980(3) Å, are comparable to other pyrrolic N−Co bonds, such as in the dipyrrolyl complex $Co_2Fe_2[(C_4H_3N)_2C(c\text{-}C_6H_{11})_2]$ (average Co−N = 2.015 Å)[19] and in the iminopyrrolyl complex $Co[(C_4H_3N)CH{=}NBu^t]_2$ (average Co−N = 1.981 Å).[22] Furthermore, the Co−imine bond lengths, Co1−N1 = 2.047(3) Å and Co1−N5 = 2.055(3) Å, are also similar to those seen in the above iminopyrrolyl complex ($Co-N_{imine}$ = 2.066 Å).[22] As with the manganese and iron helicates **2** and **3**, respectively, the cobalt helicate **4** displays asymmetry in the solid state as a consequence of intramolecular π-stacking interactions between opposing iminopyrrolyl fragments in which the pyrrolyl nitrogens N3 and N6 are separated by 3.544 Å. The formation of a

Table 2. Crystallographic Data for the Complexes **4**−**6**

	$[Co_2(L)_2]$ (**4**)	$[K_2(THF)_2(L)]$ (**5**)	$[Zn_2(L)_2]$ (**6**)
formula	$C_{42}H_{60}Co_2N_8$	$C_{52}H_{80}K_4N_8O_{2.50}$	$C_{42}H_{60}N_8Zn_2$
M_r	794.84	1013.64	807.72
cell setting, space group	orthorhombic, *Pbca*	monoclinic, $P2_1/n$	orthorhombic, *Pbca*
a (Å)	17.999(2)	14.7200(11)	17.940(3)
b (Å)	20.750(2)	26.586(2)	20.849(3)
c (Å)	21.876(2)	15.6801(12)	21.870(3)
α (deg)	90.00	90.00	90.00
β (deg)	90.00	102.2790(10)	90.00
γ (deg)	90.00	90.00	90.00
V (Å^3)	8170(2)	5995.9(8)	8180(4)
Z	8	4	8
D_x (Mg m^{-3})	1.292	1.123	1.312
μ (mm^{-1})	0.85	0.34	1.21
T_{min}, T_{max}	0.676, 1.000	0.711, 1.00	0.678, 1.000
R [$F^2 > 2\sigma(F^2)$]	0.049	0.064	0.046
wR (F^2)	0.152	0.208	0.116
S	1.08	1.04	1.02
$\Delta\rho_{max}$, $\Delta\rho_{min}$ (e Å^{-3})	0.84, −0.58	0.86, −0.53	0.73, −0.41

dinuclear cleft motif is rarely seen in dinuclear helicates but, as with **4**, is generally promoted by intrastrand π-stacking interactions.[3,5,9,23,24] For example, face-to-edge π-stacking interactions between opposing ligand strands in the dinuclear double helicate disilver bis(4,4′-quinolineiminodiphenylmethane) pull these strands together, resulting in an asymmetric helical structure.[3] In a similar manner, π-stacking interactions between opposing benzylidene rings in $Ni_2[TsNC_6H_4CH{=}N(CH_2)_3N{=}CHC_6H_4NTs]_2$ generate a similar motif.[24] In the case of **4**, only one iminopyrrolyl chelate from each ligand is employed in the π-stacking interaction and so results in a complex of overall C_2 symmetry; this feature has important consequences in the determination of the solution structures of these helicates.

Salt Elimination Routes to Dinuclear Helicates. While it is evident that the transamination reactions described above generate dinuclear double helical complexes for Mn, Fe, and Co, the difficulty in manipulating these extremely air- and moisture-sensitive precursor amides, and the surprisingly low yields observed in the case of Co, led us to investigate a more convenient entry into this chemistry using traditional salt elimination methodology. The treatment of a solution of H_2L in THF with excess KH resulted in vigorous gas evolution and the generation of the dipotassium salt $[K_2(THF)_2(L)]$ (**5**) in good yield (see Scheme 1). The ^{1}H NMR spectrum of **5** in a mixture of C_6D_6 and pyridine-d_5 is consistent with a symmetrical ligand disposition in solution, with resonances characteristic of imine, pyrrole, *meso*-methyl, and *tert*-butyl protons observed at 8.12, 6.72/6.49, 2.01, and 1.06 ppm, respectively. The coordinated THF molecules show some lability and are rapidly displaced by pyridine in solution; it was also found that they could be removed, at least partially, in the solid state under a dynamic vacuum. However, attempts to obtain a good elemental analysis for **5** have been unsuccessful, possibly because of the presence of substoichiometric amounts of THF and the sensitivity of this compound to air and moisture. X-ray-quality crystals of **5** were grown from a THF/pentane-layered solvent mixture, and the solid-state structure is shown in Figure 2, with selected bond lengths and angles described in Table 3 and crystal data in Table 2.

In the solid state, the dipotassium salt **5** adopts an infinite one-dimensional chain structure that is constructed from repeating, dimeric units of the formula $[K_2(THF)_2(L)_2]$. Each potassium has a different coordination environment: K1 adopts a distorted square-based pyramidal geometry in which the basal donors are two iminopyrrolyl chelates derived from one ligand (N1 to N4) and the axial ligand is a π-bound pyrrolyl ring (N6 and C27−C30) from the second ligand in the dimeric unit; K2 is π-bound to three pyrrolyl rings, two rings (N2, C6−C9 and N3, C13−C16) from one ligand and the second from an adjacent dimeric unit, causing the molecule to grow linearly and infinitely; K3 appears, at first sight, to adopt a distorted square-planar geometry (Σ angles at K3 = 359.8°) comprised of σ bonds to N5 and N6 of a iminopyrrolyl chelate, a π interaction with a pyrrolyl ring (N7 and C34−C37) on the same ligand, and O2 of a coordinated THF, although weak interactions between K3 and apically positioned C−H bonds from adjacent ligands are consistent with an overall pseudooctahedral coordination geometry; K4 is distorted tetrahedral with σ bonds to N7 and N8 of the iminopyrrolyl chelate and a π bond to a pyrrolyl ring (N2 and C6−C9) with the final site occupied by O1 from a THF solvent molecule. The average $K{-}N_{imino}$ (2.908 Å) and $K{-}N_{pyrrolyl}$ (2.729 Å) bond lengths of **5** are similar to those observed in K_2L^{Ph}, at 2.950 and 2.823 Å, respectively, although the $K{-}N_{imino}$ bond length in **5** is longer than that reported for the potassium salt of the bis(amidinate)

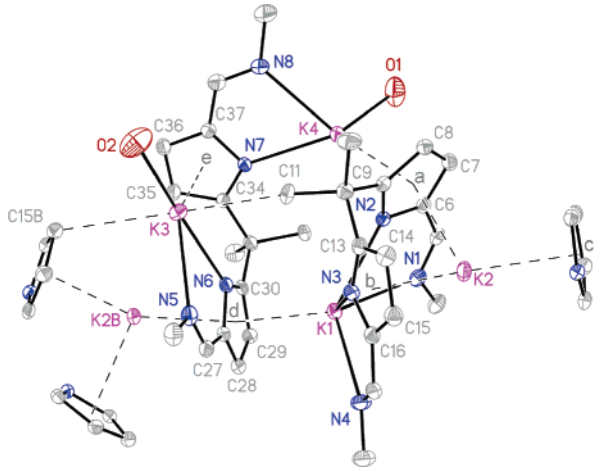

Figure 2. X-ray crystal structure of the dipotassium salt **5** (30% thermal ellipsoids; all hydrogen atoms and tert-butyl methyl and THF carbon atoms are omitted for clarity; pyrrole ring centroids are labeled a−e).

Table 3. Selected Bond Lengths (Å) and Angles (deg) for **5**

K1−N1	2.966(3)	K3−C11	3.165(3)
K1−N2	2.779(3)	K3−C15B	3.562
K1−N3	2.730(3)	N5−K3−N6	62.18(8)
K1−N4	2.948(3)	N5−K3−O2	101.94(17)
K1−d	2.955	N6−K3−e	76.6
N1−K1−N2	59.99(8)	O2−K3−e	115.5
N1−K1−N4	112.95(8)	C11−K3−C15B	172.9
N1−K1−d	119.9	K4−N7	2.728(3)
N2−K1−N3	64.72(8)	K4−N8	2.787(3)
N2−K1−d	125.8	K4−O1	2.665(3)
N3−K1−N4	61.30(8)	K4−a	2.855
N3−K1−d	124.1	N7−K4−a	128.7
N4−K1−d	112.2	N7−K4−O1	123.85(10)
K2−a	2.880	N7−K4−N8	63.91(9)
K2−b	2.893	N8−K4−O1	107.39(12)
K2−c	2.851	K2−a−K4	156.9
a−K2−b	108.6	K1−d−K2B	160.4
a−K2−c	92.6		
b−K2−c	141.7		
K3−N5	2.920(3)		
K3−N6	2.676(3)		
K3−O2	2.795(8)		
K3−e	2.933		

(19) Scott, J.; Gambarotta, S.; Yap, G.; Rancourt, D. G. *Organometallics* **2003**, *22*, 2325.
(20) Vazquez, M.; Bermejo, M. R.; Fondo, M.; Garcia-Deibe, A. M.; Sanmartin, J.; Pedrido, R.; Sorace, L.; Gatteschi, D. *Eur. J. Inorg. Chem.* **2003**, 1128.
(21) Love, J. B.; Salyer, P. A.; Bailey, A. S.; Wilson, C.; Blake, A. J.; Davies, E. S.; Evans, D. J. *Chem. Commun.* **2003**, 1390.
(22) Wei, C. H. *Inorg. Chem.* **1972**, *11*, 1100.
(23) Amendola, V.; Fabbrizzi, L.; Linati, L.; Mangano, C.; Pallavicini, P.; Pedrazzini, V.; Zema, M. *Chem.—Eur. J.* **1999**, *5*, 3679. van Stein, G. C.; van Koten, G.; Vrieze, K.; Brevard, C.; Spek, A. L. *J. Am. Chem. Soc.* **1984**, *106*, 4486.
(24) Vazquez, M.; Bermejo, M. R.; Fondo, M.; Gonzalez, A. M.; Mahia, J.; Sorace, L.; Gatteschi, D. *Eur. J. Inorg. Chem.* **2001**, 1863.

Scheme 2. Cleft Exchange Process That Occurs in Solution[a]

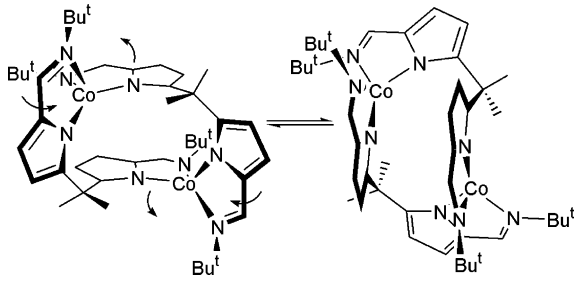

[a] No enantiomer exchange occurs as a result of this dynamic process. The *P* enantiomer is shown.

complex $K_2(THF)_5[1,2\text{-}C_6H_{10}\{NC(p\text{-tol})=N(p\text{-tol})\}_2]$, 2.781 Å;[25] this elongation can be attributed to the presence of fewer donor atoms in the latter. The average η^5-pyrrolyl−K interactions at 2.90 Å are slightly shorter than those observed for other K−dipyrrolyl ligands at 3.03 Å[26] and K−porphyrinogens at 3.048 Å.[27] However, it is important to note that both of the latter complexes also contain the extra transition-metal cations, Mo and Zr, respectively, that are also involved in bonding to the pyrrolyl groups. As with K_2L^{Ph}, the potassium cations in **5** prefer iminopyrrolyl chelation over pyrrolyl−pyrrolyl chelation. However, unlike that seen in K_2L^{Ph}, in which only the anti configuration of the pyrrolyl groups is observed, both anti and syn configurations of the pyrrolyl groups are adopted in the dimeric repeat unit of **5**.

The in situ reaction between H_2L and excess KH in THF, followed by the addition of an equimolar solution of MX_2 (MX_2 = $MnCl_2$, $FeBr_2$, and $CoCl_2$) in THF forms the [4 + 4] helicates $[M_2(L)_2]$ (M = Mn, **2**; Fe, **3**; Co, **4**) in good yield (see Scheme 1). As with the transamination routes, elemental analytical data support a 1:1 metal-to-ligand ratio in all cases, and EIMS spectra are consistent with dinuclear structures that undergo little fragmentation under electron impact conditions. It is therefore clearly evident that salt elimination reactions between K_2L and the halides of divalent Mn, Fe, and Co cleanly generate the [4 + 4] double helicates, **2**−**4**, in good yield and that this route is a good alternative to the above transamination approach.

Solution Structures of Dinuclear Helicates. To assess the stability of the dinuclear cleft motif in solution, ^{1}H NMR studies were carried out on the diiron **3** and dicobalt **4** complexes. Even though all resonances are shifted and broadened by the presence of the paramagnetic metals, it is still clear that a dynamic process occurs in solution that equilibrates both iminopyrrolyl ligand strands (see Scheme 2), as only three and four resonances were observed for **3** and **4**, respectively.

For example, the ^{1}H NMR spectrum of **3** in THF-d_8 at 298 K showed two broad resonances at 53.2 (1H) and 10.2 (ca. 8H) ppm and a very broad feature at −8.4 ppm (1H) (see Figure 3). Assignment of these resonances is difficult because it is clear that not all protons relating to L are present in the spectrum and that a dynamic process is occurring. However, cooling a sample of **3** in THF-d_8 causes these signals to coalesce at various temperatures and decoalesce into pairs that are more attributable to the C_2-symmetric structure seen in the solid state; even so, some resonances still appear absent from the low-temperature limiting spectrum. The activation barrier for the dynamic process that equilibrates the dinuclear cleft structure in **3** in solution was estimated to be $\Delta G^{\ddagger} \sim 46$ kJ mol^{-1} using values of $\Delta\upsilon$ derived from the apparent low-temperature limiting spectra of the unique protons a and b recorded at 233 and 253 K, respectively, and from approximate coalescence temperatures (T_c) of 263 and 273 K, respectively. This energy barrier is of similar magnitude to experimentally and theoretically determined binding energies for offset face-to-face π-stacking interactions between aryl groups.[28] For example, the offset face-to-face π-stacking interaction for two benzene molecules amounts to a maximum of 16 kJ mol^{-1} binding energy, approximately half of that observed for **3**.[29] However, the addition of heteroatoms such as nitrogen to the aromatic ring, and/or the extension of the aromatic π cloud such as in polyaromatic hydrocarbons, has been shown to result in a much stronger interaction.[30] It is clear that the π overlap between the two iminopyrrolyl fragments results in a relatively strong interaction (as compared to benzene), and it is therefore plausible that this cleft motif may have some influence on the unusual stability of these dinuclear helicates.[18] To assign the NMR spectra of these helicates with more confidence and to derive more accurate thermodynamic data, the diamagnetic dizinc complex, **6**, was synthesized.

The protonolysis reaction between H_2L and $ZnMe_2$ in hot toluene formed the dinuclear zinc complex, $[Zn_2(L)_2]$ (**6**), in moderate yield (see Scheme 1). This formulation is supported by elemental analysis, which is consistent with a 1:1 ligand-to-metal ratio. The EIMS spectrum of **6** showed a molecular ion at *m*/*z* 808 (60%) that is consistent with that of a dinuclear [4 + 4] helicate (calculated *m*/*z* 807.88). To confirm that **6** exhibits both double-stranded helical topology and a dinuclear cleft motif in the solid state, the X-ray crystal structure was determined on pale yellow crystals of **6** that were grown by the slow diffusion of Et_2O into CH_2Cl_2; the solid-state structure of **6** is shown in Figure 1, with selected bond lengths and angles detailed in Table 1 and crystal data in Table 2. As with the above dimanganese, diiron, and dicobalt complexes, the solid-state structure confirms the helical nature of **6** and shows that both *M* and *P* enantiomers are present in the crystal as a racemic mixture. Both Zn1 and Zn2 adopt distorted tetrahedral geometries in the solid state. The metal to imino nitrogen, Zn1−N1 = 2.054(3) Å, and metal to pyrrolyl nitrogen, Zn1−N2 = 1.978(3) Å, bond

(25) Whitener, G. D.; Hagadom, J. R.; Arnold, J. *J. Chem. Soc., Dalton Trans.* **1999**, 1249.
(26) Guohua, G.; Korobkov, I.; Gambarotta, S. *Inorg. Chem.* **2004**, *43*, 1108.
(27) Jacoby, D.; Floriani, C.; Chiesi-Villa, A.; Rizzoli, C. *J. Am. Chem. Soc.* **1993**, *115*, 7025.
(28) Hunter, C. A.; Lawson, K. R.; Perkins, J.; Urch, C. J. *J. Chem. Soc., Perkin Trans. 2* **2001**, 651. Hunter, C. A.; Saunders, J. K. M. *J. Am. Chem. Soc.* **1990**, *112*, 5525. Janiak, C. *J. Chem. Soc., Dalton Trans.* **2000**, 3885.
(29) Sinnokrot, M. O.; Sherrill, C. D. *J. Phys. Chem. A* **2003**, *107*, 8377. Sinnokrot, M. O.; Sherrill, C. D. *J. Am. Chem. Soc.* **2004**, *126*, 7690.
(30) Mignon, P.; Loverix, S.; Geerlings, P. *Chem. Phys. Lett.* **2005**, *401*, 40.

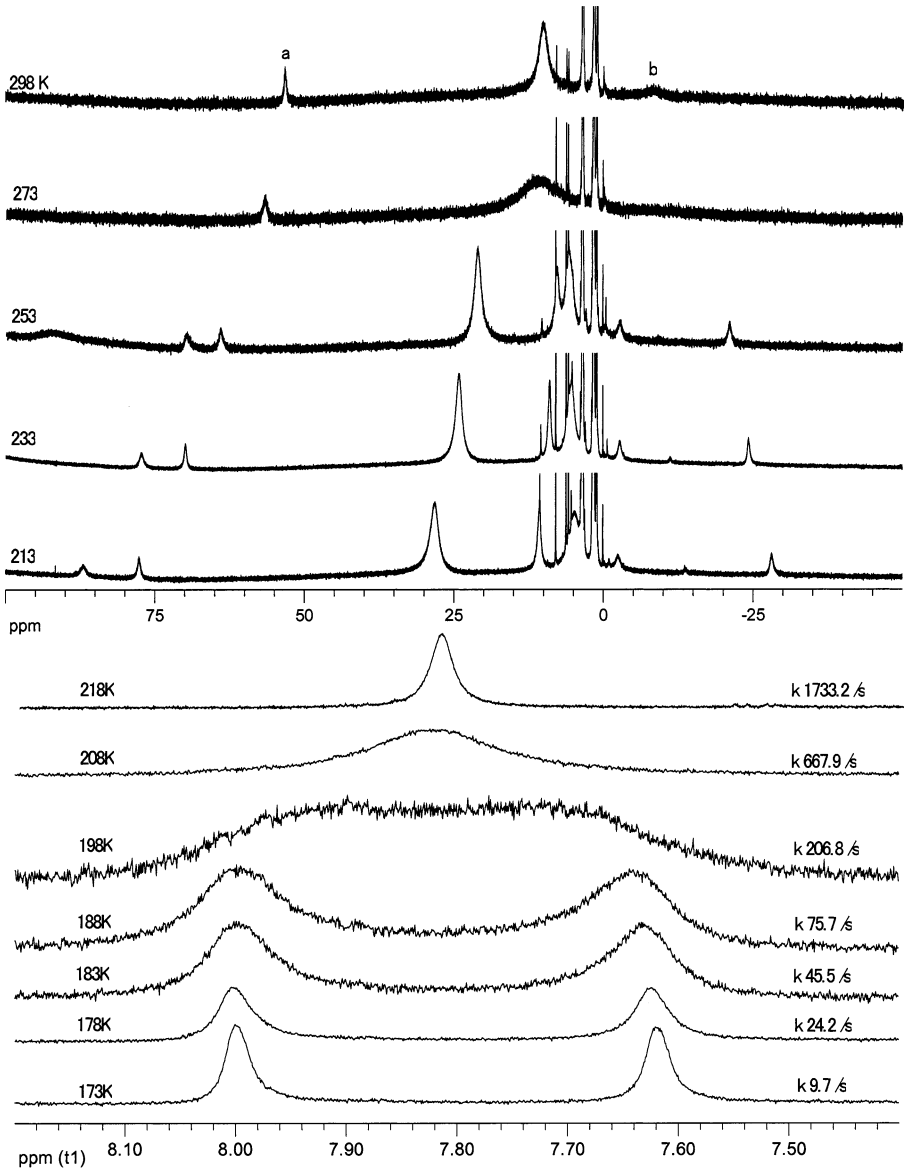

Figure 3. Variable-temperature ^{1}H NMR spectrum of **3** (top, THF-d_8) and **6** (bottom, imine region only, CD_2Cl_2).

lengths are similar to those reported previously for tetrahedral zinc complexes supported by iminopyrrolyl chelates (Zn−N_{imine} = 2.063 Å and Zn−$N_{pyrrole}$ = 1.998 Å).[14,31] However, as with **2**−**4**, the internal angle N2−Zn1−N6 at 132.08(11)° is considerably more obtuse than those observed previously for dizinc helical complexes of simple iminopyrrolyl ligands such as $Zn_2[\{(C_4H_3N)CH{=}NCH_2\}_2]$ (119.76°) and $Zn_2[\{(C_4H_3N)CH{=}NCH_2CH_2\}_2]$ (126.07°).[13] As with **2**−**4**, the metal−metal separation of 4.689 Å is long and indicative of no Zn−Zn interaction. Furthermore, it is evident that π-stacking interactions between opposing iminopyrrolyl fragments have resulted in an overall asymmetric structure, with a distance of 3.557 Å (N3−N6) separating the two iminopyrrolyl planes.

As with **3** and **4**, the asymmetry observed for **6** in the solid state is not reflected in solution. The ^{1}H NMR spectrum of **6** in CD_2Cl_2 at 298 K shows resonances that are consistent with a symmetrical ligand arrangement, and it is therefore clear that a rapid interchange between structures of D_2 and C_2 symmetry is occurring (see Scheme 2). As with **3**, this dynamic process was investigated further by variable-temperature ^{1}H NMR spectroscopy, and the results are shown in Figure 3 (bottom; only the imine region of the spectra is shown). Upon incremental cooling of **6** in CD_2Cl_2, coalescence of all proton environments is observed and results in the doubling of all resonances at the low-temperature limiting spectrum at 173 K; this is consistent with the formation of the asymmetric structure seen in the solid state that results from dinuclear cleft formation. The spectra were analyzed by line-shape simulation using WinDNMR-Pro,[32] and the exchange rate constants, k, were calculated at each temperature. A plot of $\ln(k/T)$ versus $1/T$ was linear ($R^2 = 0.9969$), from which the enthalpic $\Delta H^{\ddagger} = 33.6$ kJ mol^{-1} and entropic $\Delta S^{\ddagger} = -27.0$ J mol^{-1} K^{-1} contributions were calculated; $\Delta G^{\ddagger} = 39.0$ kJ mol^{-1} was determined for the coalescence

(31) Hao, H.; Bhandari, S.; Ding, Y.; Roesky, H. W.; Magull, J.; Schmidt, H.-G.; Noltemeyer, M.; Cui, C. *Eur. J. Inorg. Chem.* **2002**, 1060.

(32) Reich, H. J. *J. Chem. Educ. Software* **1996**, *3D*, 2.

temperature of 198 K. This energy barrier to structural symmetrization (C_2 to D_2) in **6** is very similar to that approximated for **3** and so suggests that dinuclear cleft formation is independent of the metal cation and is more likely a consequence of the overall ligand design; this is also consistent with the solid-state structures of **2**−**4** and **6**, which are isomorphous. The solution dynamics of dicopper double-stranded helicates have been assessed previously by variable-temperature NMR spectroscopy.[33] Here, the presence of labile Cu−N dative bonds in these systems results in facile ligand dissociation in solution and exchange between *M* and *P* enantiomers; exchange barriers in the range of 50.6−73.4 kJ mol^{-1} have been observed and were found to depend on the ligand design and choice of solvent. However, ligand dissociation in **2**−**4** and **6** is precluded by the presence of strong, covalent bonding between the metal cations and the charge-delocalized, uninegative iminopyrrolyl chelates. In these cases, no *M* and *P* enantiomer exchange is observed in solution, and the lack of ligand dissociation means that solvent choice is likely to have little impact on the dynamic process involving cleft formation; furthermore, the cleft-forming exchange process does not promote enantiomer exchange. We have therefore developed a series of dinuclear double-stranded helicates that adopt the same molecular structure but incorporate metals of diverse electronic properties; hence, we anticipate that these complexes will exhibit different reactivity patterns.

Conclusions

We have shown that transamination, protonolysis, and salt elimination routes can be used to synthesize Mn, Fe, Co, and Zn dinuclear [4 + 4] helical complexes of the diiminodipyrrolyl ligand L. These helicates are unusual in that they are neutral and volatile and exhibit asymmetry in the solid state that is derived from π-stacking interactions between opposing iminopyrrolyl fragments. In solution, a dynamic process exists that equilibrates this motif with energy barriers of ~46 and 39.0 kJ mol^{-1} for the iron and zinc complexes, respectively. We are currently investigating the effect that chiral imine substituents have on the preferential formation of mesocates and/or single-enantiomer helicates and also the potential of these dinuclear helicates to act as catalysts in atom-transfer reactions.

Experimental Section

Unless otherwise stated, all reactions were carried out using standard Schlenk techniques under an atmosphere of nitrogen or in a nitrogen-filled Vacuum Atmospheres OmniLab glovebox. Solvents were dried (hexane, pentane, toluene, Et_2O, and THF were passed through activated alumina towers; dichloromethane was distilled from CaH_2) and stored over 4-Å molecular sieves. Deuterated benzene and THF-d_8 were boiled over K and vacuum-distilled; pyridine-d_5 and CD_2Cl_2 were dried over activated alumina and vacuum-distilled. Solvents used in the preparation of the ligands **1** and H_2L were used as purchased. The compounds $Me_2C(C_4H_4N)_2$,[34] **1**, H_2L,[17] $Co(THF)_2[N(SiMe_3)_2]_2$,[35] **2**, and **3**[18] were synthesized according to literature procedures. The transition-metal salts $CoCl_2 \cdot 6H_2O$ and $MnCl_2 \cdot 4H_2O$ were dried according to literature procedures;[36] all other reagents were used as purchased. The ^1H and $^{13}C\{^1H\}$ NMR spectra were recorded on a Bruker DPX-300 spectrometer operating at 300.13 and 75.47 MHz, respectively; residual protiosolvent served as an internal reference for the former. Unless otherwise stated, all spectra were recorded at 298 K. Combustion analyses were carried out by Stephen Boyer at the London Metropolitan University and EIMS by Dr. Ali Abdul-Sada of the University of Sussex.

Crystallography. General Methods and Solution and Refinement Details. All single-crystal diffraction data were collected using graphite-monochromated Mo Kα X radiation on either a Bruker SMART1000 (**4**) or SMART APEX (**5** and **6**) CCD area detector diffractometer equipped with an Oxford Cryostream cooling device. All data were collected at 150 K. Details of the individual data collections and refinements are given in Table 2. All structures were solved using SHELXS-97 using heavy-atom methods for **4** and **6** and direct methods for **5**. All structures were refined by least-squares full-matrix refinement against F^2 using SHELXL-97,[37] and all fully occupied non-hydrogen atoms were refined with anisotropic atomic displacement parameters (adps). Hydrogen atoms were geometrically placed and refined as part of a riding model. **5** showed disorder in two *tert*-butyl groups, C18 and C39, which modeled over two sites with occupancies of 0.60 and 0.40 in both cases. The THF molecules containing O6S and O11S also showed disorder and were modeled over two sites with occupancies for the two sites of 0.45 and 0.55 and 0.65 and 0.55, respectively. Geometric and rigid bond restraints were applied in all cases, and partially occupied atom sites were refined with isotropic adps.

(a) Synthesis of $[Mn_2(L)_2]$ (2). To a stirred slurry of KH (88 mg, 2.20 mmol) in THF (5 mL) was added a solution of H_2L (300 mg, 0.88 mmol) in THF (10 mL). Effervescence occurred immediately, and the resulting slurry was stirred for 1 h, after which the ligand salt was added dropwise to a slurry of $MnCl_2$ (110 mg, 0.88 mmol) in THF (5 mL). The resulting yellow mixture was heated at 80 °C under reduced pressure for 24 h, after which the volatiles were evaporated at reduced pressure and the solids extracted into toluene (10 mL). The yellow slurry was filtered, and the remaining dark solid was washed with toluene (2 × 5 mL) and filtered. The toluene portions were combined, the volatiles were removed under reduced pressure, and the resultant yellow solid was washed with pentane (10 mL) to yield 158 mg, 46% of **2** as a yellow powder.

Anal. Calcd for $C_{42}H_{60}N_8Mn_2$: C, 64.10; H, 7.70; N, 14.24. Found: C, 64.11; H, 7.61; N, 14.25. EIMS: *m/z* 786 (M^+, 100), 771 ($M^+ - Me$, 47), 378 ($MnL^+ - Me$, 32).

(b) Synthesis of $[Fe_2(L)_2]$ (3). To a stirred slurry of KH (88 mg, 2.20 mmol) in THF (5 mL) was added a solution of H_2L (300 mg, 0.88 mmol) in THF (10 mL). Effervescence occurred immediately, and the resulting slurry was stirred for 1 h, after which the ligand salt was added dropwise to a slurry of $FeBr_2$ (190 mg, 0.88 mmol) in THF (5 mL). The resultant red-brown slurry was heated at 80 °C under reduced pressure for 24 h, after which the mixture was filtered, the residues were washed with THF (5 mL), and the combined filtrates were evaporated under reduced pressure. The resultant orange solid was washed once with pentane (10 mL) to yield 213 mg (61%) of **3** as an orange powder.

(33) Carina, R. F.; Williams, A. F.; Piguet, C. *Helv. Chim. Acta* **1998**, *81*, 548.
(34) Littler, B. J.; Miller, M. A.; Hung, C.-H.; Wagner, R. W.; O'Shea, D. F.; Boyle, P. D.; Lindsey, J. S. *J. Org. Chem.* **1999**, *64*, 1391.
(35) Burger, H.; Wannagat, U. *Monatsh. Chem.* **1963**, *94*, 1007.
(36) Boudjouk, P.; So, J.-H. *Inorg. Synth.* **1992**, *29*, 108.
(37) *SHELXTL*, version 6.10; Bruker AXS Inc.: Madison, WI, 2000.

Anal. Calcd for $C_{42}H_{60}N_8Fe_2$: C, 63.95; H, 7.68; N, 14.21. Found: C, 64.00; H, 7.80; N, 13.99. EIMS: *m*/*z* 788 (M^+, 100), 773 ($M^+ - Me$, 15), 325 ($L^+ - Me$, 43%). $\mu_{eff} = 7.50\ \mu_B$. ^1H NMR (THF-d_8): δ_H 53.2 (br s, 1H), 10.2 (br s, ca. 8H), −8.4 (vbr s, 1H).

(c) Synthesis of [$Co_2(L)_2$] (4). To a stirred slurry of H_2L (250 mg, 0.73 mmol) in toluene (10 mL) was added a solution of $Co(THF)_2[N(SiMe_3)_2]_2$ (384 mg, 0.73 mmol) in toluene (10 mL). The resulting maroon slurry was heated at 80 °C under reduced pressure for 24 h, after which the product slurry was filtered and the filtrate evaporated under reduced pressure. The resulting maroon solid was washed once with pentane (10 mL) to yield 12 mg (4.1%) of **4** as a red powder.

Anal. Calcd for $C_{42}H_{60}N_8Co_2$: C, 63.45; H, 7.62; N, 14.10. Found: C, 63.61; H, 7.71; N, 13.95. EIMS: *m*/*z* 794 (M^+, 91), 779 ($M^+ - Me$, 55), 749 ($M^+ - 3Me$, 50), 382 [$Co(L^1)^+ - Me$, 42], 340 (H_2L^+, 75), 325 ($H_2L^+ - Me$, 100). $\mu_{eff} = 5.12\ \mu_B$.

(d) Alternative Synthesis of 4. To a stirred slurry of KH (88 mg, 2.20 mmol) in THF (5 mL) was added a solution of H_2L (300 mg, 0.88 mmol) in THF (10 mL). Effervescence occurred immediately, and the resulting slurry was stirred for 1 h, after which the ligand salt was added dropwise to a solution of $CoCl_2$ (114 mg, 0.88 mmol) in THF (5 mL). The resulting red-brown mixture was heated at 80 °C under reduced pressure for 24 h, after which the volatiles were removed at reduced pressure and the solids extracted into CH_2Cl_2 (10 mL). The red slurry was filtered, the filtrate was evaporated at reduced pressure, and the maroon residues were washed with pentane (10 mL) to yield 0.189 g (54%) of **4** as a red powder.

EIMS: *m*/*z* 794 (M^+, 100), 779 ($M^+ - Me$, 80), 382 [$Co(L^1)^+ - Me$, 37]. $\mu_{eff} = 5.50\ \mu_B$. ^1H NMR ($CDCl_3$): δ_H 72.4 (vbr s, ca. 1H), 42.6 (br s, 1H), −35.5 (br s, 12H), −58.2 (br s, ca. 1H).

(e) Synthesis of [K_2(THF)(L)] (5). To a stirred slurry of KH (124 mg, 3.09 mmol) in THF (10 mL) at 0 °C was added a solution of H_2L (0.500 mg, 1.47 mmol) in THF (10 mL). Effervescence was observed immediately, and the reaction mixture was allowed to stir for 1 h. The resulting slurry was filtered by cannula and the pale yellow filtrate concentrated, layered with hexane (10 mL), and cooled, which resulted in the deposition of 248 mg (40%) of **5** as colorless crystals.

^1H NMR (C_6D_6/Py-d_5): δ_H 8.12 (s, 2H, N=CH), 6.80 (d, 2H, pyrrole H), 6.49 (d, 2H, pyrrole H), 2.01 (s, 6H, CH_3), 1.06 (s, 18H, CH_3). $^{13}C\{^1H\}$ NMR (C_6D_6/Py-d_5): δ_C 153.2 (s, N=CH), 146.8 (s, C_q), 116.5 (s, CH), 104.8 (s, CH), 55.2 (s, C_q), 40.4 (s, CH_3), 32.0 (s, C_q), 31.1 (s, CH_3). The other C_q's were obscured by solvent. Several attempts to obtain accurate elemental analyses were unsuccessful.

(f) Synthesis of [$Zn_2(L)_2$] (6). To a stirred slurry of H_2L (0.3 g, 0.88 mmol) in toluene (10 mL), was added dropwise a solution of $ZnMe_2$ in toluene (5 mL, 0.2 M). Effervescence occurred immediately, and the solution turned yellow. The reaction was heated at 80 °C under reduced pressure for 24 h, after which the solvents were evaporated under reduced pressure and the residues washed with pentane (5 mL) to yield 0.145 g (41%) of **6** as a pale yellow powder.

Anal. Calcd for $C_{42}H_{60}N_8Zn_2$: C, 62.44; H, 7.50; N, 13.87. Found: C, 62.68; H, 7.64; N, 13.96. ^1H NMR (CD_2Cl_2): δ_H 7.84 (s, 2H, N=CH), 6.53 (d, 2H, pyrrole H), 6.14 (d, 2H, pyrrole H). 1.56 (s, 6H, CH_3), 1.10 (s, 18H, CMe_3). $^{13}C\{^1H\}$ NMR (CD_2Cl_2): δ_C 156.3 (s, C_q), 155.5 (s, N=CH), 135.6 (s, C_q), 118.5 (s, CH), 109.4 (s, CH), 55.8, (s, C_q), 39.3 (s, C_q), 31.0 (s, CH_3), 30.9 (s, CH_3). EIMS: *m*/*z* 808 (M^+, 60), 793 ($M^+ - Me$, 35), 751 ($M^+ - Bu^t$, 23), 43 ($^tBu^+ - Me$, 100).

Acknowledgment. We thank the Royal Society (University Research Fellowship to J.B.L.), the University of Nottingham, and the EPSRC for support.

Supporting Information Available: X-ray crystallographic files for **4**−**6** (CIF). This material is available free of charge via the Internet at http://pubs.acs.org.

IC051433B